Dynamics and Structure Development During High-Speed Melt Spinning of Nylon 6. II. Mathematical Modeling

RAJEN M. PATEL, JAYENDRA H. BHEDA,* and JOSEPH E. SPRUIELL†

Department of Materials Science and Engineering and Center for Materials Processing, University of Tennessee, Knoxville, Tennessee 37996-2200

SYNOPSIS

A mathematical model of the melt spinning process that includes crystallization has been used to compute the velocity, diameter, temperature, and birefringence as a function of distance from the spinneret. An improved inversion procedure is described and is shown to give better results for the computed apparent elongational viscosity and heat-transfer coefficient data. The computed profiles have been compared directly to the experimental profiles determined earlier and reported in Part I of this paper. The results show that the model describes the major features of the melt spinning process. The reasons for the observed differences between experimental profiles and those computed from the model are discussed.

INTRODUCTION

In this paper, Part II of our study of dynamics and structure development during melt spinning of nylon 6, we describe the results of mathematical modeling of the melt spinning process and a comparison of the results to the experimental data for the two nylon 6 resins and spinning conditions studied in Part I.[1] The mathematical model used is one that was recently developed in our laboratory[2] that includes crystallization during melt spinning. The model has since been improved and implemented on an IBM PC. This model is based on earlier approaches by George,[3] Shimizu et al.,[4] and Katayama and Yoon,[5] and it allows calculation of crystallinity and birefringence profiles along the spinline as well as the effect that crystallization has on the diameter, temperature, velocity, and stress profiles.

Although there have been a number of previous attempts to model the melt spinning process, most have omitted crystallization phenomena because of the difficulties of treating nonisothermal crystallization and the effects of molecular orientation.[3,6-13] The omission of crystallization phenomena from the model made it impossible to use the earlier models to help understand how the final structure and properties of melt spun filaments are developed. This is particularly important for high-speed melt spinning as it is known that even slowly crystallizing polymers such as poly(ethylene terephthalate) will crystallize in the spinline at sufficiently high spinning speeds.[14,15] Further, our experimental results presented in Part I showed that crystallization occurs at high spinning speeds for nylon 6.[1]

Because of the existence of the experimental data of Part I, we can in the present paper compare the results of mathematical simulation directly to the experimentally measured diameter, temperature, and birefringence profiles and assess the ability of the model to simulate the experimentally observed behavior. However, the quality of predictions made by any mathematical model are highly dependent on the quality of input data. Quantities required for the present simulation include density, heat capacity, stress-optical coefficient, apparent elongational viscosity, and heat transfer coefficient. The latter two quantities are rarely known with precision, if at all. Consequently, Part I examined the possibility of using some of the on-line experimental measurements to obtain the appropriate inputs for the model. This approach has since been modified and improved upon to yield better results. The results obtained using this improved inversion procedure are pre-

* Present address: Phillips Petroleum Company, Bartlesville, Oklahoma 74004.

† To whom correspondence should be addressed.

Journal of Applied Polymer Science, Vol. 42, 1671–1682 (1991)
 CCC 0021-8995/91/061671-12$04.00

sented here and are examined in the context of the pseudoplastic nature of polymer melts. Also, an approach for evaluating the kinetics of crystallization in the presence of molecular orientation is discussed.

EXPERIMENTAL

On-line measurements for two nylon 6 homopolymer resins are compared to the simulated results in the present paper. One resin called CN 9984 had an intrinsic viscosity of 0.905 and a viscosity average molecular weight of 25,250, whereas the second resin called BHS had an intrinsic viscosity of 1.525 and a molecular weight of 53,210.

The experimental diameter profiles were measured with the aid of a Zimmer diameter monitor. The temperature profiles were measured using an infrared microscope technique, and the birefringence profiles were measured by mounting a microscope equipped with a compensator on the running spinline.

Greater detail regarding the resins and the experimental measurements of diameter, temperature, and birefringence profiles was given in our earlier paper, Part I.[1]

IMPROVED INVERSION PROCEDURE AND EVALUATION OF ELONGATIONAL VISCOSITY AND HEAT TRANSFER COEFFICIENT

An "inversion procedure" for evaluating the apparent elongational viscosity of polymer melt from spinline data was described in Part I (see Fig. 1 of Part I). The inversion procedure involves smoothing the diameter and temperature profiles using suitable fitting functions. In the analysis of Part I, the diameter profiles were directly fitted using a very high order polynomial (of 8–10th order). This high-order polynomial was necessary to accommodate the flattened diameter profile in the bottom half of the spinline. However, this procedure leads to spurious "bumps" in the calculated elongation rate profile in the bottom half and, hence, to a scatter in the apparent elongational viscosity data. This can be seen in figure 10 of Part I. Thus, a better smoothing procedure is necessary to reduce the scatter and to yield better results.

Such flattened diameter profiles are also obtained in isothermal gravity spinning experiments as reported by Patel and Bogue.[16] They successfully used a polynomial fit of reciprocal diameter $(1/D)$ vs. spinline distance to obtain the apparent elongational viscosity data. In fact, the generalized sine function fitting of the diameter data based on the isothermal Newtonian low-speed spinning theory developed by Patel and Bogue[16,17] gave results identical to those based on empirical polynomial fitting of $(1/D)$ vs. spinline distance. Hence, based on these literature results, a modified inversion procedure involving a polynomial fit of $(1/D)$ vs. spinline distance (of 4–6th order) can be used to calculate the elongation rates and the apparent elongational viscosity. The same experimental data used in Part I were reanalyzed using this modified inversion procedure. The plot of computed apparent elongational viscosity data as a function of reciprocal absolute temperature for BHS and CN9984 resins resulting from this reanalysis is shown in Figure 1.

First of all, it can be observed from Figure 1 that the resulting viscosity data are considerably smoother than the previous calculations.[1,18] This is due mainly to better smoothing of diameter data using a polynomial fit of reciprocal diameter profile and the resulting accurate calculation of the elongation rate profile. The improvement probably results from a favorable change in the error distribution and statistical weights of the data points compared to the previous procedure. The viscosity data near the die may not be accurate because of die-flow effects and also because error in the measured takeup force would give a larger error in the calculation of rheological force near the die.

It can also be seen that the computed values are somewhat different for different mass throughput rates even though each viscosity function follows nearly the Arrhenius temperature dependence. Similar differences were also obtained for results at different speeds for each throughput rate. In all the cases examined, a higher apparent elongational viscosity at a given temperature corresponded to a lower instantaneous elongation rate or stress. The reason for the difference may be attributed to the fact that most polymers, including nylon 6, exhibit non-Newtonian (deformation-thinning) viscoelastic behavior and their viscosities depend on their instantaneous deformation rate and deformation histories apart from temperature. It is interesting to note that such differences (though not large) are obtained for nylon 6 even though nylons exhibit Newtonian behavior in shear over a broad shear rate range. The scatter in the calculated viscosity data as shown in figure 10 of Part I masked the systematic differences that we have now observed using the improved procedure.

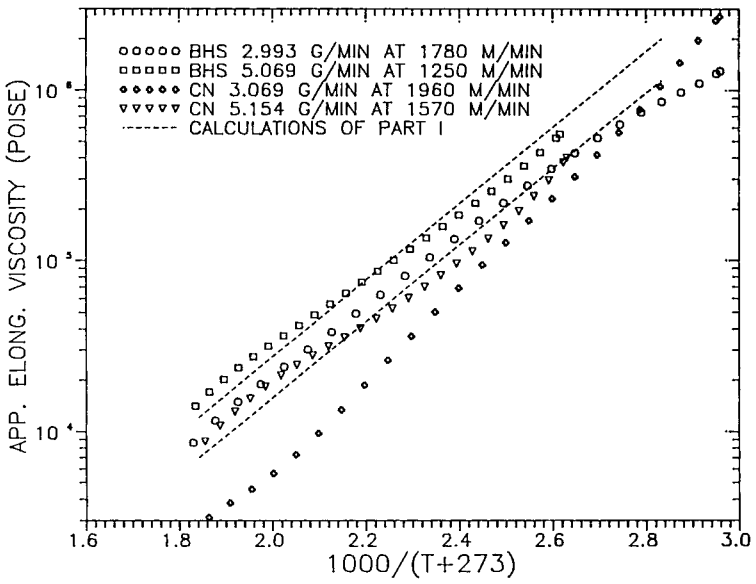

Figure 1 Calculated apparent elongational viscosity using improved inversion procedure for BHS and CN 9984 resins, each for two throughput rates.

As noted in Part I, the gradient of temperature profile can be used to evaluate the heat transfer coefficient along the spinline. For smoothing the temperature data, a second-degree polynomial fitting of temperature vs. distance data was used. The results for both the resins for two throughput rates are plotted in Figure 2. It can be observed that the data for four different cases fall on a straight line as would be desired. The calculated correlation for the heat transfer coefficient is

$$\text{HTC} = 9.287 \times 10^{-5}\left[\frac{\text{Vel}}{\text{Area}}\right]^{0.287} \quad (1)$$

Such an "inversion procedure" is very helpful as it gives values of the extensional viscosity for a given

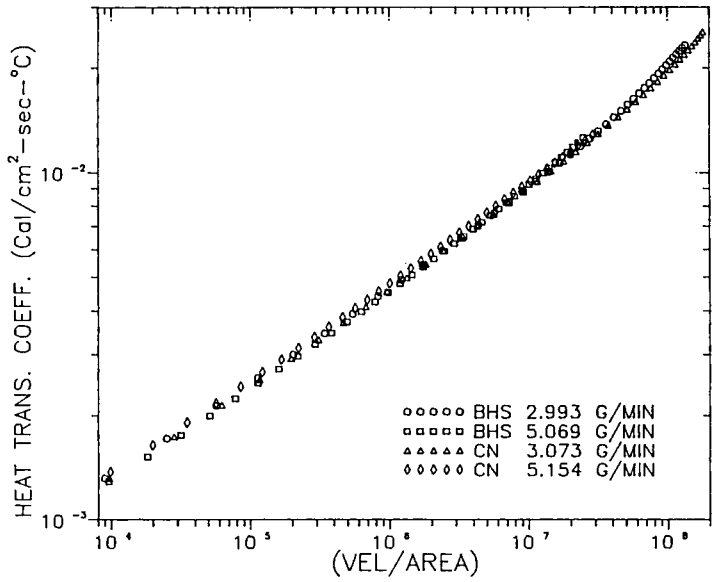

Figure 2 Calculated heat transfer coefficient correlation using improved inversion procedure for BHS and CN 9984 resins, each for two throughput rates.

resin and heat transfer coefficient data for a given experimental setup. Also, using the computed stress profile and measured birefringence profile, the stress-optical coefficient can be calculated.

The differences in computed apparent elongational viscosity data are disregarded in the present model calculations, and the Newtonian viscosity model is assumed. The required Arrhenius temperature-dependent equations were obtained from averaging the data of Figure 1. The resulting expressions for apparent elongational viscosity in poise are for CN9984:

$$\eta = 0.404 \exp\left[\frac{5140}{T + 273}\right] \tag{2}$$

and for BHS:

$$\eta = 3.517 \exp\left[\frac{4470}{T + 273}\right] \tag{3}$$

These results will be used as input parameters to the spinline model, instead of the literature values. The effect of crystallinity on viscosity is very difficult to quantify. It was assumed to be of the form (4)

$$\eta(T, X_c) = \eta(T) \exp\left[4\left(\frac{X_c}{X_\infty}\right)^2\right] \tag{4}$$

EVALUATION OF CRYSTALLIZATION KINETICS

For crystallization under quiescent, nonisothermal conditions, assuming isokinetic condition and neglecting secondary crystallization, Nakamura et al.[19] have proposed the following equation:

$$\frac{X(t)}{X_\infty} = 1 - \exp\left[-\left(\int_0^t K(T)\, dt\right)^n\right] \tag{5}$$

where $X(t)$ is the degree of phase transformation at time t, n is the Avrami index determined in the isothermal experiments, and $K(T)$ is related to the isothermal crystallization rate through the relation $K(T) = k(T)^{1/n}$. In many instances of modeling, a differential form of Eq. (5) is useful, as shown below:

$$\frac{dX(t)}{dt} = nKX_\infty(1 - \theta)\left[\ln\left(\frac{1}{1 - \theta}\right)\right]^{\frac{n-1}{n}} \tag{6}$$

For many polymers, it is possible to measure quiescent isothermal crystallization rates only over a narrow temperature range, at low supercoolings. Thus, the experimentally obtained macroscopic rate of crystallization needs to be extrapolated to lower temperatures (high supercoolings) where crystallization occurs in processing of semicrystalline polymers. Therefore, one needs an expression, preferably based on a theory, for temperature dependence of crystallization rate.

Ziabicki[20] has proposed an empirical equation for the temperature dependence of the experimentally observed crystallization half-times $t_{1/2}$ (a measure of crystallization rate) as follows:

$$\left(\frac{1}{t_{1/2}}\right) = \left(\frac{1}{t_{1/2}}\right)_{\max} \exp\left[-4 \ln(2) \frac{(T - T_{\max})^2}{D^2}\right] \tag{7}$$

where $T_{\max}$, $(1/t_{1/2})_{\max}$ and D can be determined from the isothermal crystallization kinetics experiments, using a nonlinear regression method.

Using a theoretical approach, it can be shown that $(1/t_{1/2})$ is proportional to linear growth rate G, if the number of heterogeneous nuclei is assumed to be relatively independent of temperature. The temperature variation of $t_{1/2}$ can then be written using Hoffman–Lauritzen theory[21,22] as follows:

$$\left(\frac{1}{t_{1/2}}\right) = \left(\frac{1}{t_{1/2}}\right)_0 \exp\left[-\frac{U^*}{R(T - T_\infty)}\right] \exp\left[-\frac{C_3}{T\Delta Tf}\right] \tag{8}$$

This expression can be used to obtain the value of C_3 from the slope of $\ln(1/t_{1/2}) + U^*/R(T - T_\infty)$ vs. $1/(T\Delta Tf)$ from quiescent isothermal experiments.[23] The correction factor f is usually close to 1 and can be neglected. The half-times can then be extrapolated to lower temperatures, and the Avrami rate constant k can be calculated using $k = \ln(2)/(t_{1/2})^n$. The half-time analysis approach described here is a rigorous method to evaluate quiescent kinetics of a given resin. The approach has been demonstrated for polypropylenes.[23]

Polymer crystallization is very sensitive to molecular orientation in the amorphous regions in addition to the thermal conditions. Ziabicki (20) has presented a phenomenological analysis of orientation dependence of crystallization rate and has proposed that $K(T, f_a) = K(T)\exp(Cf_a^2)$. The temperature-dependent parameter $C(T)$ can be determined from independent experiments such as by

Alfonso et al.[24] for PET, or it can be determined from spinning data.

Following Katayama and Yoon[5] and Zhou and Spruiell,[25] the following equation is proposed here in an extension of half-time analysis to include orientation effects:

$$\left(\frac{1}{t_{1/2}}\right) = \left(\frac{1}{t_{1/2}}\right)_0 \exp\left[-\frac{U^*}{R(T-T_\infty)}\right] \times \exp\left[-\frac{C_3}{T\Delta Tf + CT^2 f_a^2}\right] \quad (9)$$

The quiescent kinetics data of a given resin can then be used in a spinline model using the proposed extension of half-time analysis. Such an approach will especially be suitable for fast crystallizing polymers. The overall scheme for evaluating stress-induced crystallization from quiescent crystallization and melt spinning data is illustrated in Figure 3.

The above-mentioned empirical equations for describing stress-induced crystallization are based on an average value of amorphous orientation in the melt. Thus, they neglect the orientation distribution of amorphous segments and the effects of "selective" orientation-dependent crystallization on the orientation distribution of remaining amorphous segments.

Since quiescent crystallization kinetics data were not available for the nylons studied, estimates of

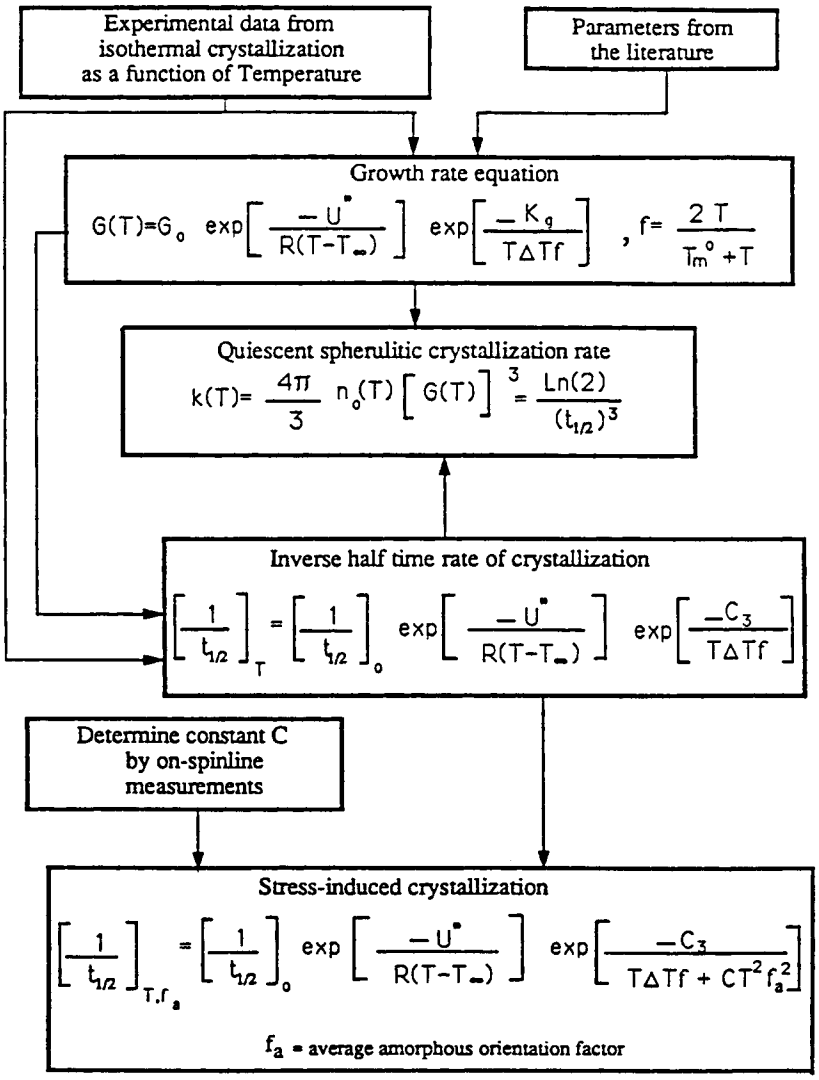

Figure 3 Scheme for evaluating stress-induced crystallization rate from quiescent crystallization and melt spinning data.

these quantities were made from the literature values of quiescent crystallization data for nylon 6 provided by Ziabicki.[20] For a slowly crystallizing polymer such as nylon or PET, literature values of the quiescent data may be sufficient and can be used in the spinline modeling for our particular nylon resins. Also, the Ziabicki term $\exp(Cf_a^2)$ is used in this paper to describe stress-induced crystallization.

DESCRIPTION OF THE MODEL AND INPUT DATA

The mathematical model used in this study was previously described in detail.[2] In the present version, the model ignores radial variations in the filament, heat conduction along the spinline, radiant heat transfer, viscous heating, and the surface tension of the polymer/air interface. Application of the kinematics of melt spinning, together with these assumptions, to the equations of continuity, momentum, and energy balance leads to a set of working relationships for the model. Also included in the working relationships are equations that describe the rheological behavior of the polymer, as well as its orientation development and crystallization kinetics. As discussed earlier, in the present calculations of the model, we assume that the rheological behavior of the polymer may be described in terms of a Newtonian constitutive equation. The crystallization kinetics are described in terms of the differential form of the Nakamura model (6) with a temperature- and molecular orientation-dependent rate parameter K from Eq. (7) and the Ziabicki term $\exp(Cf_a^2)$. It is assumed that the molecular orientation in the amorphous polymer melt can be computed from the rheo-optical law. The resulting equations that must be solved simultaneously to mathematically simulate the melt spinning process are summarized in Figure 4. The simulation was carried out using key relationships obtained from the inversion procedure and the literature values of other physical parameters. The solution procedure is based on an iterative scheme in which initial rheological force is varied until the takeup velocity condition is satisfied.

As noted above, it is necessary to have a considerable amount of input of physical property data for the model. The density (g/cc) of nylon 6 was considered to be temperature and crystallinity dependent[26]:

$$\rho = \frac{1}{[(0.8816 + 5.64 \times 10^{-4} \times T) - (0.0292 + 3.26 \times 10^{-4} \times T) \times X_c]} \quad (10)$$

The heat capacity (cal/g/°C) was taken to be[27]

$$C_p = 3.229 \times 10^{-4}(T + 273) + 0.4739 \quad (11)$$

The correlation for air drag coefficient, C_d, was taken to be $C_d = 0.27\ \mathrm{Re}^{-0.61}$.[4,28] For nylon 6, the stress optical coefficient, C_{op}, was computed from on-line measurements using the inversion procedure. The value obtained was $C_{op} = 1.2 \times 10^{-10}$ cm^2/dyne. Shimizu et al.[4] have reported $C_{op} = 0.9 - 1.8 \times 10^{-10}$ cm^2/dyne from on-line measurements. The intrinsic amorphous birefringence, Δ_a, and intrinsic crystalline birefringence, Δ_c, were considered to be constant at values of $\Delta_a = 0.0825$ and $\Delta_c = 0.0963$.[29] The heat of fusion was taken as 45 cal/g.[20] The crystalline orientation factor was assumed to be $f_c = 0.9$. The ultimate crystallinity (X_∞) was assumed to be 45%.

RESULTS AND DISCUSSION

The results of the modeling for BHS resin for two throughput rates are compared with the experimental diameter, temperature, and birefringence profiles in Figures 5–7. In these figures, the plotted points are the experimental measurements, whereas the curves represent the calculations from the model. As can be seen from these figures, the model predictions match the experimental data quite well. Similar comparisons for CN9984 resin at a lower throughput rate are shown as Figures 8–10. Again, the model predictions match the experimental data quite well. The computed crystallinity profiles for CN9984 resin are shown in Figure 11. The computed temperature profiles to illustrate the effects of mass throughput rate and the resin molecular weight are shown in Figure 12.

The predicted and the experimentally measured takeup forces are compared in Tables I and II for BHS and CN 9984 resins, respectively. The predicted values match the experimental takeup forces reasonably well. It can be seen from Figures 7 and 10 that, for each resin at lower throughput rate, predicted birefringence values are higher than are the experimental data. This may be because of using averaged viscosity in the model calculation. This led to using higher viscosities for lower throughput rates, resulting in higher spinline stresses and higher amorphous birefringence. The higher birefringence values predicted for the cases of on-line crystallization may also partially be due to higher assumed values of crystalline birefringence contribution. The similar discrepancies observed in Tables I and II may also be due to taking averaged elongational viscosity in the model calculations, resulting in higher predicted takeup tension for the lower throughput

1. **CONTINUITY**

$$W = (\pi D^2/4)\rho V$$

$$V(0) = V_o \text{ with } D(0) = D_o$$

2. **MOMENTUM BALANCE**

$$dF_{rheo}/dz = W\, dV/dz + 1/2\, \rho_a\, C_d\, V^2\, \pi D - W\, g/V$$

$$F_{rheo(0)} = ? \text{ (Guess)}; \quad C_d = k\, Re^{-n}$$

3. **ENERGY BALANCE**

$$\frac{dT}{dz} = -\frac{\pi Dh(T - T_a)}{WC_p} + \frac{\Delta H_f}{C_p}\frac{dX}{dz}$$

$$T(0) = T_o$$

4. **RHEOLOGICAL CONSTITUTIVE EQUATION**

$$\sigma = F_{rheo}/(\pi D^2/4)$$

$$\frac{dV}{dz} = \frac{\sigma}{\eta(T)}; \quad \eta(T) = A \exp\left[\frac{B}{T + 273}\right] \exp\left[a\left(\frac{X}{X_\infty}\right)^b\right]$$

5. **BIREFRINGENCE AND ORIENTATION**

$$\Delta n_a = C_{op}\, \sigma \qquad f_a = \Delta n_a/\Delta a^o$$

$$\Delta n = (1-\theta)\Delta n_a + \theta f_c \Delta c^o$$

6. **CRYSTALLIZATION KINETICS**

$$\frac{d\theta}{dz} = \frac{nK}{V}(1 - \theta)\left[\ln\left(\frac{1}{1-\theta}\right)\right]^{\frac{n-1}{n}} \qquad \text{where } \theta = \frac{X(t)}{X_\infty}$$

$$\theta(0) = 0$$

$$K(T, f_a) = (\ln 2)^{\frac{1}{n}}\left(\frac{1}{t_{1/2}}\right)_o \exp\left[-\frac{U^*}{R(T - T_\infty)}\right]\exp\left[-\frac{C_3}{T\Delta T + CT^2 f_a^2}\right]$$

OR

$$K(T, f_a) = K_{max}\, \exp\left[-4\ln(2)\frac{(T - T_{max})^2}{D^2} + Cf_a^2\right]$$

Figure 4 Summary of the working relationships of the melt spinning model.

cases. A higher value of air drag coefficient may also be a contributing factor. It can be seen that the model did not predict "necking" or sudden diameter drawdown observed for both the resins at the lower mass throughput rate at the highest spinning speeds.

The stress-induced crystallization parameter, $C = 225$, was used in these simulations. The parameter C characterizes the enhancement of crystallization rate due to orientation. The value of the parameter C as incorporated in the model for nylon 6 predicts whether crystallization will occur on-line, and if it occurs, where on the spinline it is triggered. Because of the above-mentioned limitations of the empirical equations describing stress-induced crystallization, crystallization rates are overpredicted in the later stages of crystallization. This was manifested in the prediction of a much higher temperature rise by the model than of the temperature rise experimentally observed at high spinning speeds. Similar observations were also made for polypropylenes at higher spinning speeds.[30] Therefore, in the above calculations, the crystallization rate was not allowed to exceed 10,000 sec^{-1}. This is equivalent to assuming that the crystallization rate saturates at this value. The Avrami index $n = 1$ was used in the calculations. Different values of index n did not affect the calculations as previously noted by Zieminski and Spruiell.[2]

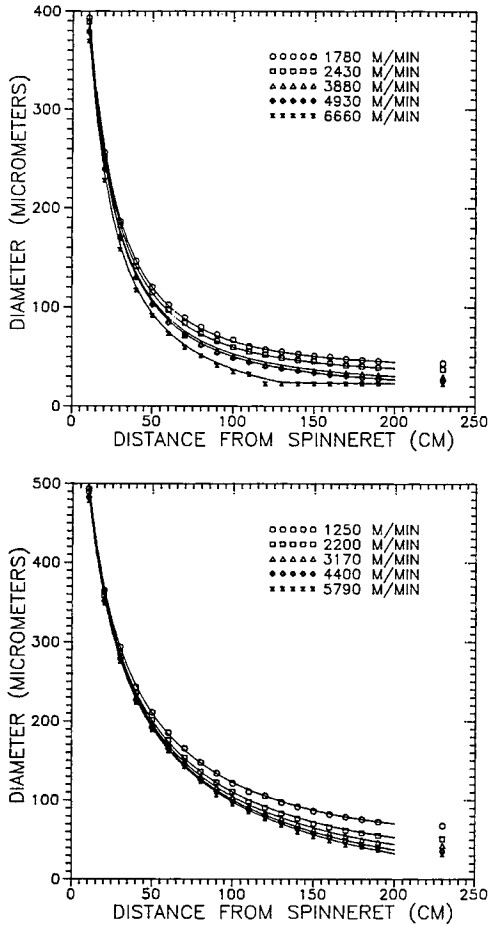

Figure 5 Comparison of the model predictions with the on-line diameter measurements for BHS resin melt spun with a mass throughput of (a) 2.993 g/min, (b) 5.069 g/min.

The simulated and the experimental results give considerable insight into the role of various process and resin variables in controlling the structure and properties of melt spun filaments. Figures 8–11 show the computed and the experimental velocity, temperature, birefringence, and crystallinity profiles for the lower molecular weight resin for filaments spun over a range of spinning speeds from 1960 to 7310 m/min. At the lowest spinning speed, the filament does not crystallize during spinning because of the slow crystallization kinetics of nylon 6. This is in spite of the fact that the lowest spinning speed corresponds to the slowest cooling rate through the range of temperatures where molecular mobility is sufficient for crystallization to occur. The molecular orientation, as measured by the birefringence, is also low in this sample throughout the spinpath. As the takeup velocity increases, the molecular orientation in the melt increases; this produces a very large increase in the crystallization rates and triggers crystallization in the spinline at spinning speeds above about 6000 m/min. The occurrence of crystallization during spinning is accompanied by a recalescence or plateauing in the temperature profile due to the heat of crystallization being converted to sensible heat as shown in Figure 9. Under these conditions, crystallization produces a rapid rise in the birefringence along the spinline due to oriented nucleation and growth of crystals and it causes a flattening of the velocity or diameter profiles due to the rapid increase of viscosity caused by the crystals.

The effects of polymer mass flow rate on the spinline dynamics can be observed in Figures 5–7 and is illustrated in Figure 12. Increasing the mass flow rate of the polymer through the spinneret hole at a given takeup velocity substantially reduces the polymer cooling rate and spinline stress; this lowers the rate of development of molecular orientation

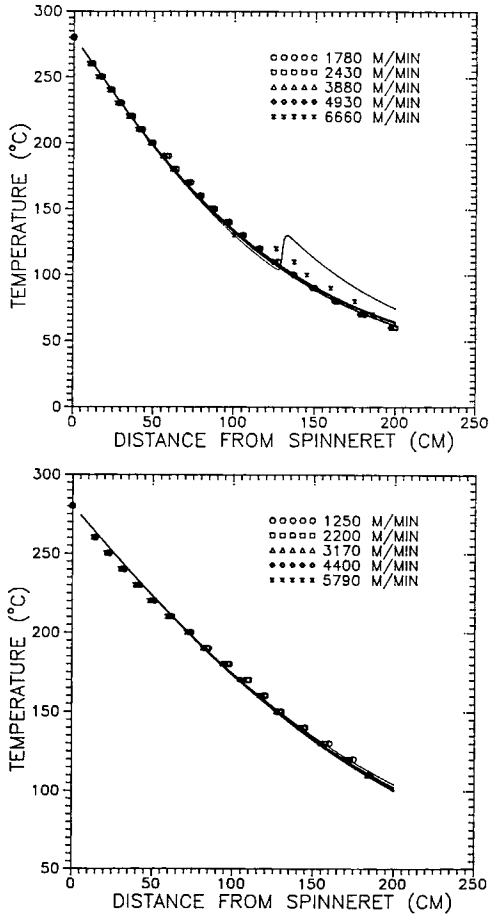

Figure 6 Comparison of the model predictions with the on-line temperature measurements for BHS resin melt spun with a mass throughput of (a) 2.993 g/min, (b) 5.069 g/min.

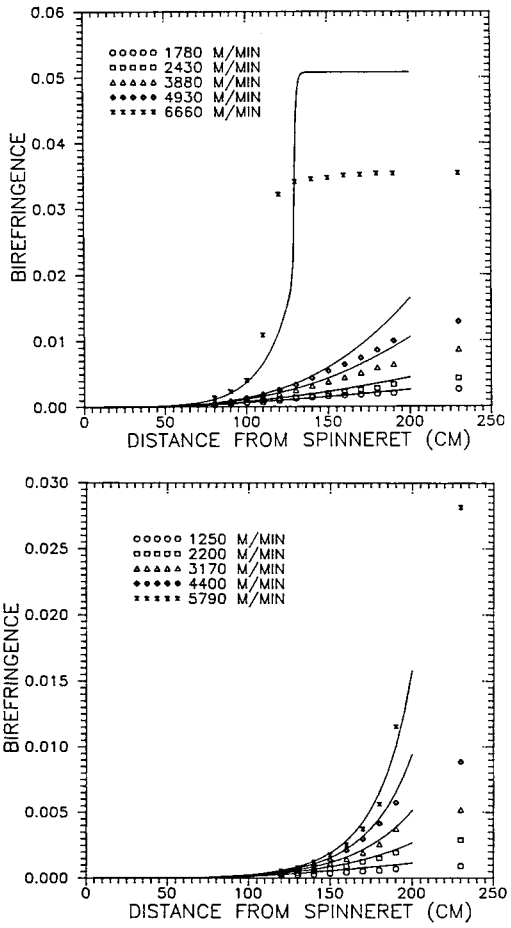

Figure 7 Comparison of the model predictions with the on-line birefringence measurements for BHS resin melt spun with a mass throughput of (a) 2.993 g/min, (b) 5.069 g/min.

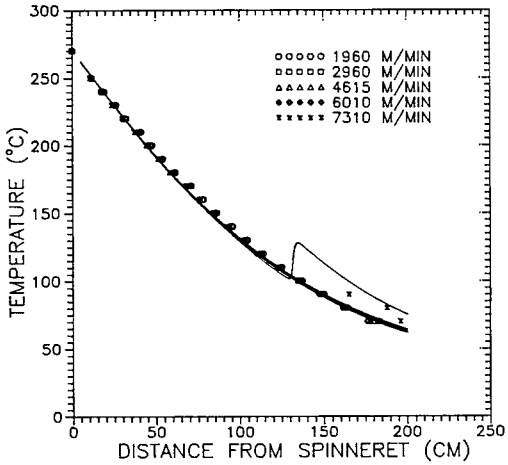

Figure 9 Comparison of the model predictions with the on-line temperature measurements for CN 9984 resin melt spun with a mass throughput of 3.069 g/min.

along the spinline and moves the point at which crystallization begins further from the spinneret. As shown in Figure 12, BHS resin spun with a mass throughput rate of 5.0 g/min and at 7000 m/min crystallizes on the spinline. However, for the same final denier filament spun at a throughput rate of 3.0 g/min, takeup velocity has to be 4180 m/min, and in that case, the filament does not crystallize on the spinline.

The effects of polymer molecular weight on spinline dynamics can also be observed in the above figures and is also illustrated in Figure 12. Increasing the polymer molecular weight for a given set of spinning conditions results in increased spinline

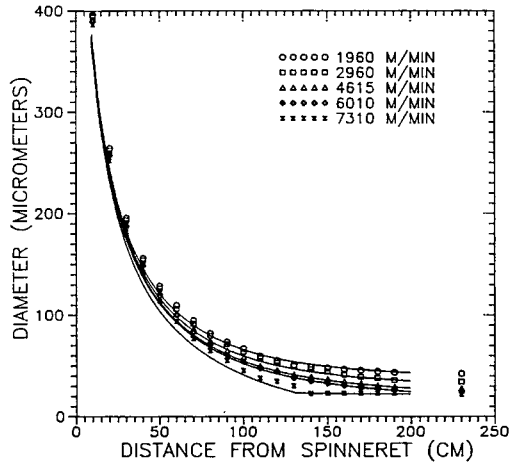

Figure 8 Comparison of the model predictions with the on-line diameter measurements for CN 9984 resin melt spun with a mass throughput of 3.069 g/min.

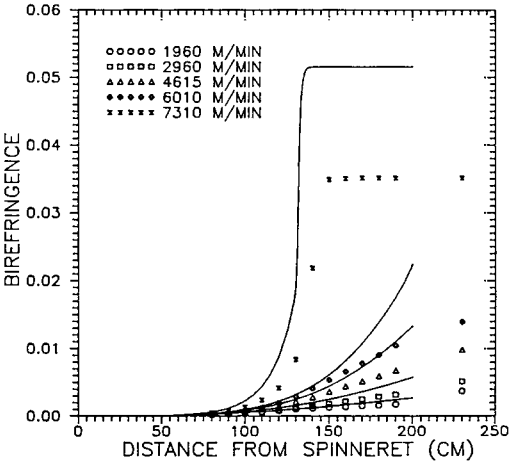

Figure 10 Comparison of the model predictions with the on-line birefringence measurements for CN 9984 resin melt spun with a mass throughput of 3.069 g/min.

stresses; this enhances the development of molecular orientation along the spinline and moves the point at which crystallization begins toward the spinneret. The effect of molecular weight on the simulated profiles is introduced through the increase in viscosity caused by the increased molecular weight.

The mathematical simulation and the experimental results make it quite clear that crystallization in the spinline is controlled by a competition between crystallization kinetics, which are largely controlled by the level of molecular orientation, and the cooling rate, which is controlled by the mass flow rate, spinning speed, and cooling medium. The balance of this competition determines whether crystallization will occur and the temperature at which it occurs. Whenever the effect of increased molecular orientation overwhelms the effect of increased cooling rate, an increase of spinning speed will result in an increase in the temperature at which crystallization occurs. But when the effect of cooling rate is more significant than is the influence of molecular orientation, the temperature of crystallization will decrease with an increase of spinning speed. If the crystallization rate becomes too low, then the polymer does not crystallize during spinning and the filament vitrifies into a glass on cooling below the glass transition temperature.

CONCLUSIONS

Because of the large number of interacting variables that affect the melt spinning process, a mathematical model of the process is quite valuable for developing an understanding of the process. An inversion procedure is useful to obtain key input relationships required for a model. The improved inversion procedure described here revealed the effects of polymer throughput rates and takeup speeds on the computed apparent elongational viscosity functions. Since the effects were not large, averaged viscosity functions were used in the present model calculations. The predictions of the mathematical model compared well with the experimental on-line measurements. The discrepancies observed can partially be attributed to the use of averaged viscosity in the model calculations.

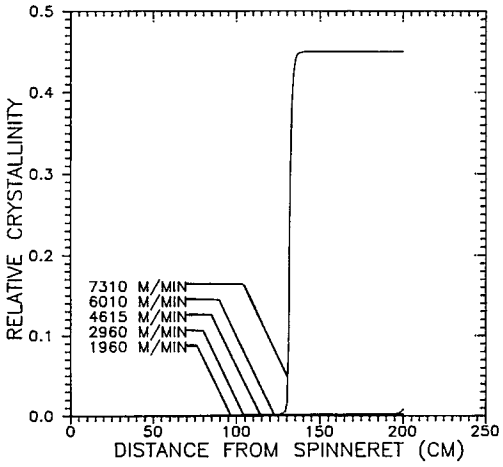

Figure 11 Computed crystallinity profiles for CN 9984 resin melt spun with a mass throughput of 3.069 g/min.

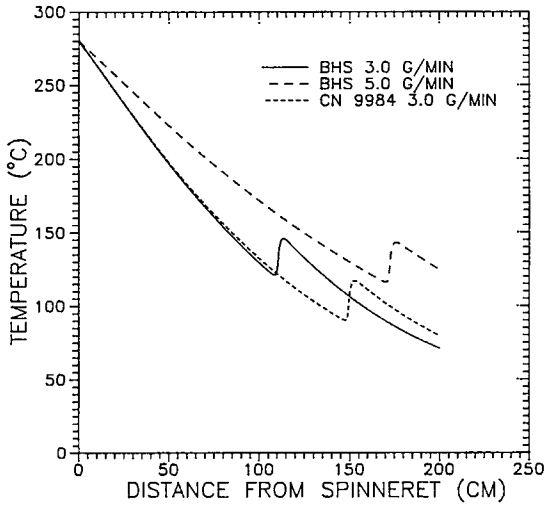

Figure 12 Effects of mass throughput rate and the resin molecular weight on the simulated temperature profiles at a takeup velocity of 7000 m/min.

The simulated and the experimental results provide considerable insight into the role of various process and resin variables in controlling the structure and properties of melt spun filaments. Increasing the mass throughput rate substantially reduces the polymer cooling rate and the spinline stress, thereby moving the point at which crystallization begins further from the spinneret. Increasing the molecular weight causes crystallization to occur closer to the spinneret and at a higher temperature.

The present simulations could not predict the "necking" observed for each resin at high speeds. Use of a non-Newtonian (deformation-thinning) constitutive equation in a spinline model probably can explain such necking phenomena. Such model is also necessary to explain the effects of throughput rate and takeup speeds on the apparent elongational viscosity function as shown by the improved inversion procedure. Crystallization rates under stress and the effect of crystallinity on viscosity are still the major areas of uncertainty in developing a better

Table I Comparison of Predicted Takeup Force with the Experimentally Measured Values for BHS Resin

BHS 2.993 g/min			BHS 5.069 g/min		
Takeup velocity (m/min)	Experimental dynes	Predicted dynes	Takeup velocity (m/min)	Experimental dynes	Predicted dynes
1780	279.3	295.6	1250	269.5	248.3
2430	347.9	382.0	2200	426.3	397.9
3880	475.3	562.8	3170	563.5	534.2
4930	553.7	685.8	4400	725.2	691.2
6660	999.6	1126.8	5790	842.8	851.3

Table II Comparison of Predicted Takeup Force with the Experimentally Measured Values for CN 9984 Resin

CN 9984 3.069 g/min			CN 9984 5.154 g/min		
Takeup velocity (m/min)	Experimental dynes	Predicted dynes	Takeup velocity (m/min)	Experimental dynes	Predicted dynes
1960	274.4	281.4	1570	284.2	256.4
2960	333.2	406.4	2560	421.4	394.1
4615	450.8	599.5	3885	588.0	554.3
6010	539.0	750.4	5180	720.3	692.6
7310	960.4	1168.5	6455	823.2	812.2

model for high-speed spinning. Further research on these aspects would enhance our understanding of many polymer processing operations.

The authors thank Allied Fibers Division of Allied Signal, Inc., for support of this research and for permission to publish the results.

REFERENCES

1. J. H. Bheda and J. E. Spruiell, *J. Appl. Polym. Sci.*, **39,** 447 (1990).
2. K. F. Zieminski and J. E. Spruiell, *J. Appl. Polym. Sci.*, **35,** 2223 (1988).
3. H. H. George, *Polym. Eng. Sci.*, **22,** 292 (1982).
4. J. Shimizu, N. Okui, and T. Kikutani, in *High Speed Fiber Spinning,* A. Ziabicki and H. Kawai, Eds., Wiley-Interscience, New York, 1985, p. 173.
5. K. Katayama and M.-G. Yoon, in *High Speed Fiber Spinning,* A. Ziabicki and H. Kawai, Eds., Wiley-Interscience, New York, 1985, p. 207.
6. S. Kase and T. Matsuo, *J. Text. Mach. Soc. Jpn.*, **18,** 188 (1965).
7. S. Kase and T. Matsuo, *J. Polym. Sci.*, **A3,** 2541 (1965).
8. S. Kase and T. Matsuo, *J. Appl. Polym. Sci.*, **11,** 251 (1967).
9. A. Prastaro and P. Parrini, *Text. Res. J.*, **45,** 118 (1975).
10. H. Yasuda, H. Sugiyama, and Y. Yanagawa, *Sen-i Gakkaishi,* **35,** 370 (1979).
11. D. K. Gagon and M. M. Denn, *Polym. Eng. Sci.*, **21,** 844 (1981).
12. H. Yasuda, H. Sugiyama, and S. Hayashi, *Sen-i Gakkaishi,* **40,** 227, 488 (1984).
13. A. Dutta and V. M. Nadkarni, *Text. Res. J.*, **54,** 35 (1984).
14. G. Perez and C. Lecluse, in *Proceedings of the 18th International Man-made Fiber Conference,* Dornbirn, Austria, 1979.
15. M. Matsui, in *High Speed Fiber Spinning,* A. Ziabicki and H. Kawai, Eds., Wiley-Interscience, New York, 1985, p. 137.
16. R. M. Patel and D. C. Bogue, *J. Rheol.*, **33**(4), 607 (1989).
17. R. M. Patel, *Ind. Eng. Chem. Res.*, **28**(12), 1910 (1989).
18. J. H. Bheda, Ph.D. Dissertation, University of Tennessee, Knoxville (1987).

19. K. Nakamura, K. Katayama, and T. Amano, *J. Appl. Polym. Sci.*, **17,** 1031 (1973).
20. A. Ziabicki, in *Fundamentals of Fiber Formation,* Wiley-Interscience, New York, 1976.
21. J. D. Hoffman and J. Weeks, *J. Chem. Phys.*, **37,** 1723 (1962).
22. J. D. Hoffman, G. T. Davis, and J. I. Lauritzen, in *Treatise on Solid State Chemistry: Crystalline and Non-crystalline Solids,* J. B. Hannay, Ed. Plenum, New York, 1976, Vol. 3, Chap. 7.
23. A. Hammami, J. Zhou, R. M. Patel, and J. E. Spruiell, in *AIChE Annual Meeting,* San Francisco, November, 1989.
24. G. C. Alfonso, M. P. Verdona, and A. Wasiak, *Polymer,* **19,** 711 (1978).
25. J. Zhou and J. E. Spruiell, in *Nonwovens—An Advanced Tutorial,* A. F. Turbak and T. L. Vigo, Eds., TAPPI Press, Atlanta, 1989, pp. 131–157.
26. M. Inoue, *J. Polym. Sci. A-1,* 2013 (1963).
27. U. Gaur, S.-F. Lau, B. B. Wunderlich, and B. Wunderlich, *J. Phys. Chem. Ref. Data,* **12,** 65 (1983).
28. M. Matsui, *Trans. Soc. Rheo.*, **20,** 465 (1976).
29. K. Matsumoto and M. Kiyodu, *Sen-i Gakkaishi,* **32,** 365 (1976).
30. R. M. Patel and J. E. Spruiell, unpublished results (1989).

Received May 10, 1990
Accepted June 19, 1990